

# RSC Advances



This is an *Accepted Manuscript*, which has been through the Royal Society of Chemistry peer review process and has been accepted for publication.

*Accepted Manuscripts* are published online shortly after acceptance, before technical editing, formatting and proof reading. Using this free service, authors can make their results available to the community, in citable form, before we publish the edited article. This *Accepted Manuscript* will be replaced by the edited, formatted and paginated article as soon as this is available.

You can find more information about *Accepted Manuscripts* in the [Information for Authors](#).

Please note that technical editing may introduce minor changes to the text and/or graphics, which may alter content. The journal's standard [Terms & Conditions](#) and the [Ethical guidelines](#) still apply. In no event shall the Royal Society of Chemistry be held responsible for any errors or omissions in this *Accepted Manuscript* or any consequences arising from the use of any information it contains.

# Preparation of Copper Doped Magnetic Porous Carbon for Removal of Methylene Blue by a Heterogeneous Fenton-like Reaction

Chao Bao<sup>1</sup>, He Zhang<sup>1</sup>, Lincheng Zhou<sup>\*</sup>, Yanming Shao, Junjun Ma, Qiong Wu

*State Key Laboratory of Applied Organic Chemistry, College of Chemistry and Chemical Engineering, Institute of Biochemical Engineering & Environmental Technology, Lanzhou University, Lanzhou 730000, P. R. China*

Chao Bao E-mail: baoch13@lzu.edu.cn Fax: 86-931-8912113 Tel. 86-931-8912528

Address: College of Chemistry and Chemical Engineering, Lanzhou University, Lanzhou 730000, P.R.China

He Zhang E-mail: zhangh12@lzu.edu.cn Fax: 86-931-8912113 Tel. 86-931-8912528

Address: College of Chemistry and Chemical Engineering, Lanzhou University, Lanzhou 730000, P.R.China

Lincheng Zhou E-mail: zhoulc@lzu.edu.cn Fax: 86-931-8912113 Tel. 86-931-8912528

Address: College of Chemistry and Chemical Engineering, Lanzhou University, Lanzhou 730000, P.R.China

Yanming Shao E-mail: shaoym11@lzu.edu.cn Fax: 86-931-8912113 Tel. 86-931-8912528

Address: College of Chemistry and Chemical Engineering, Lanzhou University, Lanzhou 730000, P.R.China

Junjun Ma E-mail: majj12@lzu.edu.cn Fax: 86-931-8912113 Tel. 86-931-8912528

Address: College of Chemistry and Chemical Engineering, Lanzhou University, Lanzhou 730000, P.R.China

Qiong Wu E-mail: qwu14@lzu.edu.cn Fax: 86-931-8912113 Tel. 86-931-8912528

Address: College of Chemistry and Chemical Engineering, Lanzhou University, Lanzhou 730000, P.R.China

---

<sup>\*</sup>Corresponding author. Tel: 86-931-8912528. E-mail: Zhoulc@lzu.edu.cn (Zhou lincheng)

<sup>1</sup>These authors contributed equally to this work.

## Abstract

High-specific-surface-area copper doped magnetic porous carbon ( $\text{CuFe}_2\text{O}_4/\text{Cu}@C$ ) was fabricated by annealing iron, copper and 1,3,5-benzenetricarboxylic ([Cu/Fe]-BTC) metal–organic coordination polymers, which were prepared via a one-pot solvothermal method. The novel  $\text{CuFe}_2\text{O}_4/\text{Cu}@C$  catalyst consists of Cu (3.80%),  $\text{CuFe}_2\text{O}_4$  (64.84%), and C (31.36%). Scanning electron microscopy, X-ray diffraction, X-ray photoelectron spectroscopy, element analysis, inductively coupled plasma, Brunauer–Emmett–Teller surface area measurement, and vibrating sample magnetometer analysis were used to characterize the materials. The as-prepared materials were employed as heterogeneous Fenton's reagent with the addition of  $\text{H}_2\text{O}_2$  for degradation of methylene blue (MB). The results showed that the materials effectively catalyzed  $\text{H}_2\text{O}_2$  to generate hydroxyl radicals ( $\bullet\text{OH}$ ). And due to their magnetism, materials can be easily separated from wastewater to realize the repeatability. It also turned out that  $\text{CuFe}_2\text{O}_4/\text{Cu}@C$  had a higher catalytic activity than  $\text{Fe}_3\text{O}_4@C$ , which proved the importance of copper doped in the catalyst. This work indicated that porous carbon composites provide good support for the development of a highly efficient heterogeneous Fenton catalyst that is useful for environmental pollution cleanup.

## 1. Introduction

Treatment and control of organic pollutants have become a priority task in the drinking water industry. However, the removal of the most organic pollutants from drinking water is a difficult task, because their odor threshold is extremely low. Only a few water treatment technologies have been successfully applied to remove organic pollutants from water including the use of physical methods<sup>1, 2</sup>, biotechnology<sup>3</sup>, and chemical technology<sup>4</sup>. However, physical methods, such as liquid–liquid extraction, ion-exchange, adsorption, and air or steam stripping, are ineffective on pollutants that are not readily adsorbed or volatile; these approaches have disadvantages because they simply transfer the pollutants to another phase rather than destroying them<sup>5</sup>. The adsorption process of activated carbon to remove organic pollutants is an recognized practice; however, the treatment cost may be costly<sup>6</sup>. Ozone and hypochlorite oxidations are efficient decolorizing methods, but they are undesirable because of the high cost of equipment, operating costs, and secondary pollution<sup>7</sup>.

Recently, Chemical treatment methods based on the generation of hydroxyl radicals, known as advanced oxidation processes (AOPs), have been recently applied for pollutant degradation because of the high oxidative power of the OH radical. These techniques generate a free hydroxyl radical ( $\bullet\text{OH}$ ) that degrades most of the organic pollutants rapidly and non-selectively. The Fenton reaction is a well-studied AOP that uses hydrogen peroxide as an oxidant in the presence of a catalyst<sup>8-10</sup>. The nonselective attack of organic compounds by the hydroxyl radicals results in mineral end-products. The classical Fenton reagent consists of a homogeneous solution of iron

ions and hydrogen peroxide. Catalysis is effective only within a low and narrow pH range. This process also produces iron sludge as a treatment byproduct, which is an additional environmental contaminant. Therefore, Heterogeneous catalysts have been developed to overcome these problems<sup>11-14</sup>. The  $\text{Fe}^{2+}$  ion in  $\text{Fe}_3\text{O}_4$  makes this compound a very efficient catalyst for the degradation of organic pollutants and allows it to be easily separated from the reaction medium using an external magnetic field. Therefore, magnetite is suitable as a heterogeneous Fenton catalyst. However, the aggregation of  $\text{Fe}_3\text{O}_4$  nanoparticles, which is the major challenge in using catalytic nanoparticles in practical application, substantially reduces catalytic efficiency<sup>15</sup>. Hence, significant efforts have been made to overcome these disadvantages<sup>10, 16, 17</sup>. Iron oxides can be immobilized in organic or inorganic supports to form the novel heterogeneous Fenton catalysts. Among the porous solids used as supports for iron phases, carbon materials, such as graphene<sup>18</sup> and activated carbon<sup>19</sup>, gained popularity because of their excellent chemical stability, mechanical strength, and large surface area. Porous carbon possesses high specific surface area that can improve the activity of iron oxide by preventing the aggregation and improving the dispersibility of the catalyst.

Metal–organic frameworks (MOFs) are crystalline materials composed of metal ions and organic ligands. The pore size and functional groups of MOFs can be adjusted given the variety of metal ions and organic ligands<sup>20</sup>. These distinct characteristics make MOFs excellent candidates for various applications, such as gas storage<sup>21, 22</sup>, chemical separation<sup>23</sup>, drug delivery<sup>24</sup>, and catalysis<sup>25</sup>. In recent years, the

utilization of MOFs as heterogeneous catalysts has received significant attention. However, the application of MOFs in special environments, such as acidic, alkali, and high-temperature environments, is limited because of their low stability. Moreover, the recycling of MOFs is a complicated task after reaction. The utilization of MOFs as templates or precursor materials to produce porous carbonaceous materials has been demonstrated because MOFs have a large surface area and possess a significant amount of carbon<sup>26, 27</sup>.

In this work, we present a facile method to synthesize  $\text{CuFe}_2\text{O}_4/\text{Cu}@C$  composite material derived from iron, copper, and 1,3,5-benzenetricarboxylic ([Cu/Fe]-BTC) metal-organic coordination polymers prepared by using a one-pot solvothermal method. Scanning electron microscopy (SEM), X-ray diffraction (XRD), Fourier transform infrared (FT-IR) spectroscopy, X-ray photoelectron spectroscopy (XPS) spectra, vibrating sample magnetometry (VSM), inductively coupled plasma atomic emission spectroscopy (ICP-AES), and Brunauer-Emmett-Teller (BET) analyses were used to characterize the magnetic porous composite material. The ability of the particles to facilitate the Fenton oxidation of methylene blue (MB) was tested under varying conditions of initial pH,  $\text{H}_2\text{O}_2$  concentration,  $\text{NH}_2\text{OH}$ , catalyst dosage concentration, MB concentration, and temperature. The stability and reusability of the magnetic porous carbon spheres were also tested. Moreover, the catalytic activity of  $\text{CuFe}_2\text{O}_4/\text{Cu}@C$  and  $\text{Fe}_3\text{O}_4@\text{C}$  were compared.

## 2. Experimental

### 2.1 Materials

$\text{Cu}(\text{NO}_3)_2$  and  $\text{FeCl}_3$  were purchased from Sinopharm Chemical Reagent Co. (Shanghai, China). Benzene-1,3,5-tricarboxylic acid ( $\text{H}_3\text{BTC}$ ) and Hydroxylamine hydrochloride ( $\text{HONH}_3\text{Cl}$ ) were purchased from Aldrich. sodium hydroxide and hydrogen peroxide were purchased from Shanghai Chemical Reagents Company. MB was supplied by Tianjin Tiantai Fine Chemicals Co., Ltd. All the chemicals were of analytical grade.

## 2.2 Synthesis of $\text{CuFe}_2\text{O}_4/\text{Cu}@C$ composite

$\text{CuFe}_2\text{O}_4/\text{Cu}@C$  composite were prepared by solvothermal method under autogenous pressure. In a typical experiment, 0.3244 g  $\text{FeCl}_3$  (2 mmol), 0.3624 g  $\text{Cu}(\text{NO}_3)_2$  (1.5 mmol) and 0.6305 g  $\text{H}_3\text{BTC}$  (3 mmol) were firstly dissolved in 20 mL ethanol under vigorous stirring for 30 min. Then the mixture was sealed in a 60 mL Teflon-lined stainless-steel autoclave and heated at  $78^\circ\text{C}$  for 8 h. After that, the autoclave was carefully removed and allowed to cool to room temperature. The as-synthesized polymer was washed by ethanol several times and centrifuged and then dried at  $60^\circ\text{C}$  in vacuum for 12h. The dried polymer powder was obtained. Finally, the resulting powder was annealed at the temperature of  $500^\circ\text{C}$  in nitrogen atmosphere for 3 h. After cooling to room temperature, the as-prepared  $\text{CuFe}_2\text{O}_4/\text{Cu}@C$  composite were collected for following use.

## 2.3 Synthesis of $\text{Fe}_3\text{O}_4@C$ composite

For comparing,  $\text{Fe}_3\text{O}_4@C$  composite were also prepared by solvothermal method. In a typical experiment, 1.6220 g  $\text{FeCl}_3$  and 1.4010 g  $\text{H}_3\text{BTC}$  were dissolved in 30 mL ethanol under vigorous stirring for 30 min. The following process was just the same

as synthesis of  $\text{CuFe}_2\text{O}_4/\text{Cu}@C$  composite.

#### 2.4 Dye Decoloration through a Heterogeneous Fenton Reaction.

The catalytic property of  $\text{CuFe}_2\text{O}_4/\text{Cu}@C$  materials was explored by studying the change of the absorbance intensity at the maximum absorbance wavelength of the MB dye. Typically, 5 mg resulting catalysts were added to 10 mL of a  $20 \text{ mg L}^{-1}$  MB solution in the presence of  $\text{H}_2\text{O}_2$  and  $\text{NH}_2\text{OH}$ , and the suspension was shaken in a thermostated shaker at 130 rpm at  $30^\circ\text{C}$ . After the reaction, the composite were separated using an external magnetic field, then the concentration of MB was determined using a UV-vis spectrometer, with a maximum absorbance wavelength for MB at 664 nm. Total organic carbon (TOC) was determined by a TOC analyzer after filtration through a  $0.45 \mu\text{m}$  membrane filter.

#### 2.7 Characterization

The morphology of the Sample was examined by scanning electron microscope (SEM, JSM-6701F, JEOL, Japan). FT-IR spectra were obtained in transmission mode on a FT-IR spectrometer (American Nicolet Corp., Model 170-SX) using the KBr pellet technique. XRD (Rigaku D/MAX-2400 X-ray diffractometer with Ni-filtered  $\text{Cu K}\alpha$  radiation ( $\lambda = 1.54056$ )) was used to investigate the crystal structure of the nanoparticles. The Fe and Cu content of the prepared nanocatalysts were obtained by inductively coupled plasma atomic emission spectroscopy (ICP-AES). Magnetization measurements at room temperature were obtained using a Vibrating sample magnetometer (LAKESHORE-7304, USA) at room temperature. The X-ray photoelectron spectroscopy (XPS) spectra were obtained with an ESCALab220i-XL

electron spectrometer (VG Scientific) using 300 W Al-K $\alpha$  radiation. The N<sub>2</sub> adsorption-desorption isotherm was measured at liquid nitrogen temperature (77 K) using a Micromeritics ASAP 2020 analyzer. The specific surface area was calculated by the BET method. The pore size distribution was obtained using the Barret-Joner-Halenda (BJH) method. UV-Vis detection was carried out on a TU-1810PC UV-Vis spectrophotometer (Purkinje General, China). TOC was determined using a TOC analyzer (Elementar vario TOC cube, Hanau, Germany).

### 3. Results and discussion

#### 3.1 Morphology and structure characterization

Solvothermal method was conducted to prepare CuFe<sub>2</sub>O<sub>4</sub>/Cu@C and Fe<sub>3</sub>O<sub>4</sub>@C composite materials under autogenous pressure. Fig. 1 shows representative SEM images of CuFe<sub>2</sub>O<sub>4</sub>/Cu@C and Fe<sub>3</sub>O<sub>4</sub>@C composites. The SEM image (Fig. 1a) shows that the Fe<sub>3</sub>O<sub>4</sub>@C composite is an amorphous state and Fe<sub>3</sub>O<sub>4</sub> crystal disperses well in the substrate (Fig. 1b, 1c). Based on Figs. 1d–1f, CuFe<sub>2</sub>O<sub>4</sub>/Cu@C composite have the same amorphous states.

PXRD analysis also provided information on the composition of the as-synthesized samples. To verify the formation of CuFe<sub>2</sub>O<sub>4</sub>/Cu@C and Fe<sub>3</sub>O<sub>4</sub>@C composites, we obtained XRD patterns of [Cu/Fe]-BTC and Fe-BTC samples, as shown in Fig. 2. The position of the two groups of diffraction peaks is consistent with the standard XRD data for the MIL-100 (Fe) in Figs. 2a and 2b. Results are also consistent with other findings in literature<sup>28, 29</sup>. The finding demonstrates the formation of [Cu/Fe]-BTC and Fe-BTC composites. After the carbonization process,

some diffraction peaks disappeared. As shown in Fig. 2c, the diffraction peaks of  $\text{Fe}_3\text{O}_4@\text{C}$  at  $2\theta = 30.26^\circ, 35.66^\circ, 43.22^\circ, 53.62^\circ, 57.21^\circ,$  and  $62.74^\circ$  are ascribed to (220), (311), (400), (422), (511), and (440) planes, which agree well with the standard XRD data for the cubic phase  $\text{Fe}_3\text{O}_4$  (JCPDS card, file no. 89-4319), with a face-centered cubic structure<sup>30</sup>. Result indicates the formation of the crystal  $\text{Fe}_3\text{O}_4$ . Meanwhile, the diffraction peaks of  $\text{CuFe}_2\text{O}_4/\text{Cu}@\text{C}$  at  $2\theta = 30.17^\circ, 35.58^\circ, 43.36^\circ, 53.52^\circ, 57.21^\circ, 62.67^\circ,$  and  $74.22^\circ$  were ascribed to (220), (311), (400), (422), (511), (440), and (533) planes, which agree with the standard XRD data for  $\text{CuFe}_2\text{O}_4$  (JCPDS card, file no. 77-0010). However, the diffraction peaks at  $2\theta = 43.36^\circ$  and  $74.22^\circ$  were particularly strong, and an additional diffraction peak appeared at  $2\theta = 50.54^\circ$ . As stated in a previous report<sup>31</sup>, the diffraction peaks at  $2\theta = 43.36^\circ, 74.22^\circ,$  and  $50.54^\circ$  belong to (111), (200), and (220) planes, which agree well with  $\text{Cu}^0$  (JCPDS card, file no. 70-3039). This result indicates that the  $\text{CuFe}_2\text{O}_4/\text{Cu}@\text{C}$  composite was formed.

EA and ICP-AES analyses determined the chemical composition of the composite.  $\text{Fe}_3\text{O}_4@\text{C}$  consists of Fe (30.61%) and C (37.37%), and  $\text{CuFe}_2\text{O}_4/\text{Cu}@\text{C}$  consists of Cu (19.31%), Fe (21.84%), and C (31.36%). The relative molar ratio of Cu to Fe was 0.88 based on the quantitative analyses. This result is consistent with that of XRD and confirm the existence of  $\text{Cu}^0$ .

XPS was employed to investigate the chemical state of the surface of the obtained  $\text{Fe}_3\text{O}_4@\text{C}$  and  $\text{CuFe}_2\text{O}_4/\text{Cu}@\text{C}$ . Fig. S1a exhibits the overall survey of the as-synthesized  $\text{Fe}_3\text{O}_4@\text{C}$  composite and clearly shows the signals of elemental C, O,

and Fe. Fig. S1a evidently illustrates that the signal of C is significantly stronger than those of other elements (i.e., O and Fe) on the catalyst surface. This phenomenon results from the carbonization process. In addition, Fig. S1b shows the XPS spectra of Fe 2p spectrum. The Fe 2p spectrum can be deconvoluted into two peaks centered at 725.2 and 711.1 eV, which correspond to the peaks of Fe 2p<sub>1/2</sub> and Fe 2p<sub>3/2</sub>. Meanwhile, the Fe 2p<sub>3/2</sub> spectrum was resolved into three peaks at 710.0, 711.1, and 712.4 eV, which compared well with Fe<sup>2+</sup> octahedral species, Fe<sup>3+</sup> octahedral species, and Fe<sup>3+</sup> tetrahedral species. In addition, the Fe 2p<sub>1/2</sub> spectrum has the same regulation. The position of the Fe 2p peaks corresponds to that of Fe<sub>3</sub>O<sub>4</sub><sup>32</sup>. Fig. S1c shows the XPS spectra of O 1s, which can be deconvoluted into three peaks centered at 529.9, 531.6, and 533.1 eV that correspond to C-O, C=O, and O-C=O species. Fig. S1d shows the XPS spectra of C 1s, which also prove the existence of C-O, C=O, and O-C=O species. Fig. S2 shows the overall survey of CuFe<sub>2</sub>O<sub>4</sub>/Cu@C composite, which clearly indicates the signals of elemental C, O, Cu, and Fe. Figs. S2b and S2c show the XPS spectra of C 1s and O 1s that verify the existence of C-O, C=O, and O-C=O species. The Fe 2p spectrum (Fig. S2d) can be deconvoluted into two peaks centered at 725 and 710 eV, which correspond to the peaks of Fe 2p<sub>1/2</sub> and Fe 2p<sub>3/2</sub>. Meanwhile, the Fe 2p<sub>3/2</sub> (Fe 2p<sub>1/2</sub>) spectrum was resolved into two peaks at 710.9 and 712.9 eV (724.5 and 727.4 eV), which compared well with Fe<sup>3+</sup> octahedral species and Fe<sup>3+</sup> tetrahedral species. Fig. S1e shows the XPS spectra of the Cu 2p spectrum. The Cu 2p<sub>3/2</sub> (Cu 2p<sub>1/2</sub>) can be deconvoluted into three peaks centered at 933.9, 935.2, and 931.9 eV (953.6, 955.1, and 951.6 eV), which compared well with Cu<sup>2+</sup>

octahedral species,  $\text{Cu}^{2+}$  tetrahedral species, and  $\text{Cu}^0$ , respectively<sup>33, 34</sup>. This result also confirms the existence of  $\text{Cu}^0$ .

The BET surface area was measured using the  $\text{N}_2$  adsorption/desorption isotherms at  $-197.2$  °C. Prior to measurements, the samples were evacuated at  $100$  °C for 10 h. The BET surface areas (Fig. 3) of  $\text{Fe}_3\text{O}_4@\text{C}$  and  $\text{CuFe}_2\text{O}_4/\text{Cu}@\text{C}$  were  $168.95$  and  $160.74$   $\text{m}^2/\text{g}$ , respectively. The high BET surface areas of the catalyst supports should be useful in pollutant removal by increasing the contact frequency between the pollutants and catalyst. The inset figures show that the pore size distribution curve of  $\text{Fe}_3\text{O}_4@\text{C}$  and  $\text{CuFe}_2\text{O}_4/\text{Cu}@\text{C}$ . The adsorption average pore width of them were  $4.31$  and  $2.11$  nm, respectively. The two composites exhibited a significant difference in the pore size distribution because of the  $\text{Cu}^0$  block part of the channel pore.

The magnetic properties of the resultant core-shell microspheres were investigated at room temperature with vibrating sample magnetometry in the field range of  $-10$  kOe to  $10$  kOe (Fig. 4). The magnetization saturation values of  $\text{Fe}_3\text{O}_4@\text{C}$  and  $\text{CuFe}_2\text{O}_4/\text{Cu}@\text{C}$  were  $41.84$  and  $33.36$  emu/g, respectively. The measured values indicated the strong magnetic properties of the prepared catalysts. All of the curves present a magnetic hysteresis loop that confirms the strong magnetic response to a varying magnetic field. Furthermore,  $\text{Fe}_3\text{O}_4@\text{C}$  and  $\text{CuFe}_2\text{O}_4/\text{Cu}@\text{C}$  indicated ferromagnetic-type curves that show a hysteresis loop. The values of coercivity and remanence are summarized in Table 1. The rapid aggregation of the catalysts can be observed from their homogeneous dispersion in the presence of an

external magnetic field applied for 20 s. This observation directly demonstrates the convenient separation of catalysts through an external magnetic field, which is important in practical manipulation.

### 3.2 Catalytic Properties of Magnetic Porous Carbon composite

To prove that copper doped can improve catalytic activity, we subsequently selected  $\text{CuFe}_2\text{O}_4/\text{Cu}@C$  for further analysis as a catalyst for MB degradation. The ability of  $\text{CuFe}_2\text{O}_4/\text{Cu}@C$  to remove MB was tested in different systems (Fig. 5). Adding the  $\text{CuFe}_2\text{O}_4/\text{Cu}@C$  composite to a MB solution resulted to almost 18.2% MB removal, which was likely due to adsorption only. Using the  $\text{CuFe}_2\text{O}_4/\text{Cu}@C$  composite in the presence of both  $\text{NH}_2\text{OH}$  and  $\text{H}_2\text{O}_2$  led to the removal of nearly all of the MB within 30 min. The degradation of MB was compared using pristine  $\text{Fe}_3\text{O}_4$ <sup>35</sup>, prepared by traditional coprecipitation.  $\text{CuFe}_2\text{O}_4/\text{Cu}@C$  composite performed more efficiently than the unmodified  $\text{Fe}_3\text{O}_4$  using similar dosages of the catalyst. Conversely, when  $\text{NH}_2\text{OH}$  and  $\text{H}_2\text{O}_2$  were added into the MB solution without  $\text{CuFe}_2\text{O}_4/\text{Cu}@C$  composite, only 2% of the MB was removed because of the free radicals formed by  $\text{H}_2\text{O}_2$  in the presence of the reducing reagent  $\text{NH}_2\text{OH}$ <sup>36</sup>. This result suggests that the  $\text{CuFe}_2\text{O}_4/\text{Cu}@C$  composite helped degrade MB through adsorption, thus improving the reaction rate.

The progress of MB degradation can be easily followed by the decrease in absorbance at  $\lambda_{\text{max}}$  (664 nm) of MB with time. Fig. 6 shows the successive UV-vis spectra of MB in the presence of the  $\text{CuFe}_2\text{O}_4/\text{Cu}@C$  composite,  $\text{H}_2\text{O}_2$ , and  $\text{NH}_2\text{OH}$  in aqueous solution. The adsorption band decreased rapidly and disappeared in 30 min

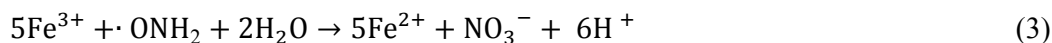
without the appearance of new adsorption bands in the visible or ultraviolet regions. This observation indicates that the benzene ring and heteropolyaromatic linkages of MB were likely destroyed and MB was almost completely degraded. Therefore, pseudo-first order kinetics on the degradation of MB, described as  $\ln(C/C_0) = -kt$ , can be applied to better understand the MB degradation reaction kinetics.  $C$  is the concentration of MB at time  $t$ ,  $C_0$  is the initial concentration of MB, and  $k$  is the rate constant that can be calculated from the slope of the straight line. Inset in Fig. 6 reveals the linear relationship between  $\ln(C/C_0)$  and the reaction time  $t$ , which matches well with the first-order reaction kinetics. The rate constant  $k$  of MB degradation was calculated to be  $0.1094 \text{ min}^{-1}$  at  $30 \text{ }^\circ\text{C}$  with  $\text{CuFe}_2\text{O}_4/\text{Cu}@C$  composite. The calculated value is significantly higher than the literature reported value of  $2.35 \times 10^{-3} \text{ min}^{-1}$  using titanomagnetite as the heterogeneous catalyst<sup>37</sup> and  $5.73 \times 10^{-2} \text{ min}^{-1}$  using FeS as the heterogeneous catalyst<sup>38</sup>.

The as-synthesized  $\text{CuFe}_2\text{O}_4/\text{Cu}@C$  composite showed excellent degradation compared with  $\text{Fe}_3\text{O}_4@\text{C}$  (Fig. 7). The dynamic degradation curve shows that the removal efficiency reached 100% within 15 min in the presence of the  $\text{CuFe}_2\text{O}_4/\text{Cu}@C$  composite. However, when  $\text{Fe}_3\text{O}_4@\text{C}$  worked as catalyst, MB degradation was only 56% within 15 min. To  $\text{Fe}_3\text{O}_4$ , the value was only 2%. Fig. 7b shows that the homogeneous solution generated more  $\bullet\text{OH}$  in the presence of the  $\text{CuFe}_2\text{O}_4/\text{Cu}@C$  composite. The result indicates the synergistic effect of the  $\text{Cu}^0$  in the generation of  $\bullet\text{OH}$ .

### 3.3 Exploration of the degradation conditions

### 3.3.1. Effect of pH

An assessment of the effects of pH was initially investigated in the presence of H<sub>2</sub>O<sub>2</sub> and NH<sub>2</sub>OH (Fig. 8a). Tests were conducted at pH 3.02, 5.12, 8.14, and 10.11. MB degradation was nearly 100% within 15 min at pH 3.02, 5.12, and 8.14. However, the removal efficiency of the composite decreased to 80% at pH 10.11. Generally, pH 3.0 is optimal for organic pollutant degradation by Fenton systems<sup>39</sup>. The best pH value for the degradation of MB in this Fenton-like system was approximately 3, as seen in Fig. 8a. This observation is consistent with the classical Fenton reaction. The classical Fenton reagent is effective only within a low and narrow pH range, but the CuFe<sub>2</sub>O<sub>4</sub>/Cu@C composite resulted in a broader range for the Fenton reaction. The degradation of MB is less efficient at a higher pH because of the instability of H<sub>2</sub>O<sub>2</sub> in an alkaline solution; the production of •OH on the surface of CuFe<sub>2</sub>O<sub>4</sub>/Cu@C composite was gradually restricted with increasing pH, which also resulted in a slower degradation rate of MB<sup>40</sup>. The process of H<sub>2</sub>O<sub>2</sub> activation by CuFe<sub>2</sub>O<sub>4</sub>/Cu@C composite is speculated to involve the following steps<sup>41-43</sup>:



### 3.3.2 Effect of H<sub>2</sub>O<sub>2</sub> concentration

Another important parameter in removing MB is the concentration of H<sub>2</sub>O<sub>2</sub>. The added amount of H<sub>2</sub>O<sub>2</sub> varied from 2.67 mmol to 10.67 mmol (Fig. 8b). The removal efficiency of MB improved as the H<sub>2</sub>O<sub>2</sub> concentration increased from 2.67 mmol L<sup>-1</sup> to 5.33 mmol L<sup>-1</sup>, but the removal efficiency did not change significantly from 5.33 mmol L<sup>-1</sup> to 10.67 mmol L<sup>-1</sup>. This observation may have occurred because H<sub>2</sub>O<sub>2</sub> could not generate a sufficient number of •OH radicals, which slowed the oxidation rate and reduced the removal efficiency at low concentrations. Higher concentrations of H<sub>2</sub>O<sub>2</sub> could generate enough •OH radicals. However, the use of excess H<sub>2</sub>O<sub>2</sub> is wasteful and costly, and this process can also reduce the efficiency because of the hydroxyl radical scavenging effect<sup>44</sup> (Eqs. 8 and 9). Hence, 5.33 mmol L<sup>-1</sup> is optimal for MB degradation by the Fenton-like system.



### 3.3.3 Effect of NH<sub>2</sub>OH concentration

NH<sub>2</sub>OH is a common reducing agent that is used to eliminate problems associated with the traditional homogenous Fenton system, such as the accumulation of Fe<sup>3+</sup> and the narrow pH range limits<sup>45</sup>. Research indicates that adding NH<sub>2</sub>OH to a Fenton-like system could accelerate the redox cycles of Fe<sup>3+</sup> to Fe<sup>2+</sup>. Hence, compared with no NH<sub>2</sub>OH, the new system notably alleviated the Fe<sup>3+</sup> accumulation, enhanced the reaction rates, and expanded the effective pH range. The generation of •OH was significantly faster because of the participation of NH<sub>2</sub>OH. In addition, the

$\text{NO}_3^-$  and  $\text{N}_2\text{O}$  were proposed as the dominant end-products of  $\text{NH}_2\text{OH}$ . Considering the excellent effects of  $\text{NH}_2\text{OH}$  in a homogenous Fenton system, we added it into a heterogeneous Fenton-like system to evaluate its synergistic effect. The added amount of  $\text{NH}_2\text{OH}$  varied from 1.67 to 6.67  $\text{mmol L}^{-1}$  (Fig. 8c). The degradation percentage of MB increased with  $\text{NH}_2\text{OH}$  concentration. When the  $\text{NH}_2\text{OH}$  concentration reached 6.67  $\text{mmol L}^{-1}$ , the removal efficiency was above 100%. These results indicate that  $\text{NH}_2\text{OH}$  also produced a positive effect in the heterogeneous Fenton-like system.  $\text{NH}_2\text{OH}$  accelerated the redox cycles of  $\text{Fe}^{3+}$  to  $\text{Fe}^{2+}$  involving the following steps:



### 3.3.4 Effect of catalyst dosage

The use of excessive catalyst is wasteful and costly; hence, the dosage of the catalyst was also evaluated using  $\text{CuFe}_2\text{O}_4/\text{Cu}@C$  composite of 0.2, 0.5, 1.0, and 1.5  $\text{g L}^{-1}$  in degradation reactions. The initial rates increased with the amount of  $\text{CuFe}_2\text{O}_4/\text{Cu}@C$  composite. The improved efficiency caused by increased catalyst loading introduced more active sites, which generated more free-radical species that promote the degradation reaction. In Fig. 8d, the removal efficiency reached 100% within 20 min when the catalyst concentration was 0.5  $\text{g L}^{-1}$ .

### 3.3.5 Effect of MB dosage

The influence of MB dosage was investigated using the MB at 20, 60, and 100  $\text{mg L}^{-1}$  (Fig. 8e). The efficiency decreased because of the increased concentration of

MB within 30 min. This result indicated that the extension of the reaction time is necessary when dealing with a large amount of organic pollutants.

### 3.3.6 Effect of the temperature

Determining the reaction rates under different temperatures is often very useful in providing insights on reaction mechanisms. Increasing temperature usually causes a significant increase in the reaction rate depending on the reaction processes. Experiments on the effect of temperature were conducted to evaluate the activation energy (Fig. 8f). An Arrhenius equation describing the relationship between rate constants and temperature was applied:

$$\ln k = -\frac{E_a}{RT} + \ln A_0$$

where  $k$  is the measured first-order rate constant,  $A_0$  is a frequency factor,  $E_a$  is the activation energy,  $R$  is ideal gas constant, and  $T$  is temperature. The activation energy for the degradation of MB was measured in a closed batch system, and temperature varied from 293 K to 313 K. The value of activation energy was 38.16 KJ/mol, which indicates that the reaction is a surface-controlled reaction<sup>46</sup>. The rate constants at different temperatures are summarized in Table 2.

### 3.4 Stability and Reuse of the Catalyst

The stability of the CuFe<sub>2</sub>O<sub>4</sub>/Cu@C composite is a critical factor for its practical applications. To evaluate the catalyst stability of the catalysts, we carried out recycling reactions for the degradation of MB. The solid catalyst was magnetically separated from the reactant mixture, washed with ethanol, and vacuum-dried at 60 °C after each catalytic cycle. The MB concentrations were detected to evaluate the

catalytic activity in the repeated process, and the initial MB concentration was 20 mg L<sup>-1</sup>. As shown in Fig. 9, the catalyst retained its original activity after 10 repeated reuses. Both the MB and TOC concentrations were detected to evaluate the catalytic activity in the repeated process. This result indicates that the efficiency of TOC removal was lower than the MB removal efficiency with each repetition; the maximum efficiency of TOC removal was 70%, whereas it was nearly 100% in MB removal. The eventual decrease of the catalytic activity may have been caused by the incomplete removal of byproducts during washing. The stability of CuFe<sub>2</sub>O<sub>4</sub>/Cu@C composite was better compared with other heterogeneous Fenton catalysts<sup>47, 48</sup>. To investigate the structure of the catalyst after the Fenton reaction, XPS was used after 10 repeated reuses (Fig. 10). The details of the Fe 2p peaks and Cu 2p peaks of the CuFe<sub>2</sub>O<sub>4</sub>/Cu@C composite before and after use during MB degradation are presented in Table 3. This result indicates the presence of one oxidation states for the surface iron species before being used. The Fe 2p<sub>3/2</sub> (Fe 2p<sub>1/2</sub>) spectrum was resolved into two peaks at 710.9 and 712.9 eV (724.5 and 727.4 eV), which compared well with Fe<sup>3+</sup> octahedral species and Fe<sup>3+</sup> tetrahedral species. For the sample after MB degradation, Fe<sup>3+</sup> was 68.6% and Fe<sup>2+</sup> was 31.4%. These values indicate that part of Fe<sup>3+</sup> in the outermost layer of the catalyst was deoxidized into Fe<sup>2+</sup> during the Fenton reaction. For the copper species, Cu 2p<sub>3/2</sub> (Cu 2p<sub>1/2</sub>) can be deconvoluted into three peaks centered at 933.9, 935.2, and 931.9 eV (953.6, 955.1, and 951.6 eV) that compared well with Cu<sup>2+</sup> octahedral species, Cu<sup>2+</sup> tetrahedral species, and Cu<sup>0</sup>, respectively. However, the percentage of Cu<sup>2+</sup> reduced from 80.3% to 60.6% after MB degradation.

Copper was involved in heterogeneous Fenton-like reaction. All of these results further indicate that the catalyst exhibited excellent durability because of the protective effects of the porous carbon support and the presence of  $\text{NH}_2\text{OH}$ .

#### 4. Conclusion

In conclusion,  $\text{CuFe}_2\text{O}_4/\text{Cu}@C$  composite was fabricated by annealing  $[\text{Cu}/\text{Fe}]\text{-BTC}$  at  $500\text{ }^\circ\text{C}$  in an inert atmosphere. The resultant composite material showed excellent catalytic performance in MB degradation and superparamagnetic behavior that enabled magnetic separation and convenient recovery from the reaction mixture. Moreover, the composite was stable and reusable, indicating that it could overcome the drawbacks of homogeneous catalysts. For comparison, the  $\text{Fe}_3\text{O}_4@C$  composite was fabricated using the same strategy. Results showed that  $\text{CuFe}_2\text{O}_4/\text{Cu}@C$  had a higher catalytic activity than  $\text{Fe}_3\text{O}_4@C$ , which proved the importance of copper doped in the catalyst. Therefore, the composite catalysts show a great potential for industrial application.

#### Acknowledgement

The authors would like to express their appreciation for research funding provided by the National Natural Science Foundation of China (Nos. 21374045, 21074049) and the National Science Foundation for Fostering Talents in Basic Research of the National Natural Science Foundation of China (Grant No. J1103307).

#### References

1. J. H. Mo, Y. H. Lee, J. Kim, J. Y. Jeong and J. Jegal, *Dyes Pigm.*, 2008, **76**, 429-434.
2. M. Rafatullah, O. Sulaiman, R. Hashim and A. Ahmad, *J. Hazard. Mater.*, 2010, **177**, 70-80.
3. C. Meehan, A. J. Bjourson and G. McMullan, *Int. J. Syst. Evol. Micr.*, 2001, **51**, 1681-1685.

4. L. Shen, P. Yan, X. Guo, H. Wei and X. Zheng, *Arab. J. Sci. Eng.*, 2014, **39**, 6659-6664.
5. K. Dutta, S. Mukhopadhyay, S. Bhattacharjee and B. Chaudhuri, *J. Hazard. Mater.*, 2001, **84**, 57-71.
6. A. Georgi and F.-D. Kopinke, *Appl. Catal. B.*, 2005, **58**, 9-18.
7. Y. Yoshida, S. Ogata, S. Nakamatsu, T. Shimamune, K. Kikawa, H. Inoue and C. Iwakura, *Electrochim. Acta.*, 1999, **45**, 409-414.
8. M. Neamțu, C. Catrinescu and A. Kettrup, *Appl. Catal. B.*, 2004, **51**, 149-157.
9. M. Pérez, F. Torrades, X. Domènech and J. Peral, *Water. Res.*, 2002, **36**, 2703-2710.
10. I. A. Salem, *Appl. Catal. B.*, 2000, **28**, 153-162.
11. A. H. Gemeay, I. A. Mansour, R. G. El-Sharkawy and A. B. Zaki, *J. Mol. Catal. A: Chem.*, 2003, **193**, 109-120.
12. V. V. Ishtchenko, K. D. Huddersman and R. F. Vitkovskaya, *Appl. Catal. A.*, 2003, **242**, 123-137.
13. S. Letaïef, B. Casal, P. Aranda, M. A. Martín-Luengo and E. Ruiz-Hitzky, *Appl. Clay Sci.*, 2003, **22**, 263-277.
14. G. Tachiev, J. A. Roth and A. R. Bowers, *Int. J. Chem. Kinet.*, 2000, **32**, 24-35.
15. S. Zhang, X. Zhao, H. Niu, Y. Shi, Y. Cai and G. Jiang, *J. Hazard. Mater.*, 2009, **167**, 560-566.
16. J. Chun, H. Lee, S.-H. Lee, S.-W. Hong, J. Lee, C. Lee and J. Lee, *Chemosphere*, 2012, **89**, 1230-1237.
17. L. Kong, X. Lu, X. Bian, W. Zhang and C. Wang, *ACS Appl. Mat. Interfaces.*, 2011, **3**, 35-42.
18. W. Liu, J. Qian, K. Wang, H. Xu, D. Jiang, Q. Liu, X. Yang and H. Li, *J. Inorg. Organomet. P.*, 2013, **23**, 907-916.
19. H. Zhao, Y. Wang, Y. Wang, T. Cao and G. Zhao, *Appl. Catal. B.*, 2012, **125**, 120-127.
20. D. Bradshaw, J. B. Claridge, E. J. Cussen, T. J. Prior and M. J. Rosseinsky, *Acc. Chem. Res.*, 2005, **38**, 273-282.
21. M. O'Keefe, M. A. Peskov, S. J. Ramsden and O. M. Yaghi, *Acc. Chem. Res.*, 2008, **41**, 1782-1789.
22. N. L. Rosi, J. Eckert, M. Eddaoudi, D. T. Vodak, J. Kim, M. O'Keefe and O. M. Yaghi, *Science*, 2003, **300**, 1127-1129.
23. C.-X. Yang, H.-B. Ren and X.-P. Yan, *Anal. Chem.*, 2013, **85**, 7441-7446.
24. P. Horcajada, T. Chalati, C. Serre, B. Gillet, C. Sebrie, T. Baati, J. F. Eubank, D. Heurtaux, P. Clayette, C. Kreuz, J.-S. Chang, Y. K. Hwang, V. Marsaud, P.-N. Bories, L. Cynober, S. Gil, G. Ferey, P. Couvreur and R. Gref, *Nat. Mater.*, 2010, **9**, 172-178.
25. B. Li, Y. Zhang, D. Ma, L. Li, G. Li, G. Li, Z. Shi and S. Feng, *Chem. Commun.*, 2012, **48**, 6151-6153.
26. W. Cho, S. Park and M. Oh, *Chem. Commun.*, 2011, **47**, 4138-4140.
27. X. Yan, X. Li, Z. Yan and S. Komarneni, *Appl. Surf. Sci.*, 2014, **308**, 306-310.
28. T. D. Bennett and A. K. Cheetham, *Acc. Chem. Res.*, 2014, **47**, 1555-1562.
29. S. Shahid and K. Nijmeijer, *J. Membr. Sci.*, 2014, **459**, 33-44.
30. B. Li, H. Cao, J. Shao, M. Qu and J. H. Warner, *J. Mater. Chem.*, 2011, **21**, 5069-5075.
31. L. Chen, Y. Shen, J. Bai and C. Wang, *J. Solid State Chem.*, 2009, **182**, 2298-2306.
32. D. Wilson and M. A. Langell, *Appl. Surf. Sci.*, 2014, **303**, 6-13.
33. C. Reitz, C. Suchomski, J. Haetge, T. Leichtweiss, Z. Jaglicic, I. Djerdj and T. Brezesinski, *Chem. Commun.*, 2012, **48**, 4471-4473.
34. Y. Wang, H. Zhao, M. Li, J. Fan and G. Zhao, *Appl. Catal. B.*, 2014, **147**, 534-545.

35. Z. L. Liu, Y. J. Liu, K. L. Yao, Z. H. Ding, J. Tao and X. Wang, *J. Mater. Synth. Process.*, 2002, **10**, 83-87.
36. S. Y. Wang and H. Jiao, *J. Agric. Food. Chem.*, 2000, **48**, 5677-5684.
37. S. Yang, H. He, D. Wu, D. Chen, Y. Ma, X. Li, J. Zhu and P. Yuan, *Ind. Eng. Chem. Res.*, 2009, **48**, 9915-9921.
38. A. K. Dutta, S. K. Maji, D. N. Srivastava, A. Mondal, P. Biswas, P. Paul and B. Adhikary, *ACS Appl. Mat. Interfaces.*, 2012, **4**, 1919-1927.
39. S. M. Arnold, W. J. Hickey and R. F. Harris, *Environ. Sci. Technol.*, 1995, **29**, 2083-2089.
40. F. Ji, C. Li, J. Zhang and L. Deng, *Desalination*, 2011, **269**, 284-290.
41. L. Chen, J. Ma, X. Li, J. Zhang, J. Fang, Y. Guan and P. Xie, *Environmental Science & Technology*, 2011, **45**, 3925-3930.
42. J. Lind and G. Merényi, *The Journal of Physical Chemistry A*, 2006, **110**, 192-197.
43. X. Zhang, Y. Ding, H. Tang, X. Han, L. Zhu and N. Wang, *Chemical Engineering Journal*, 2014, **236**, 251-262.
44. C. Walling, *Acc. Chem. Res.*, 1975, **8**, 125-131.
45. L. Chen, J. Ma, X. Li, J. Zhang, J. Fang, Y. Guan and P. Xie, *Environ. Sci. Technol.*, 2011, **45**, 3925-3930.
46. H.-L. Lien and W.-X. Zhang, *Appl. Catal., B*, 2007, **77**, 110-116.
47. T. D. Nguyen, N. H. Phan, M. H. Do and K. T. Ngo, *J. Hazard. Mater.*, 2011, **185**, 653-661.
48. M. Zhu and G. Diao, *J. Phys. Chem. C.*, 2011, **115**, 18923-18934.

## Figures and Tables

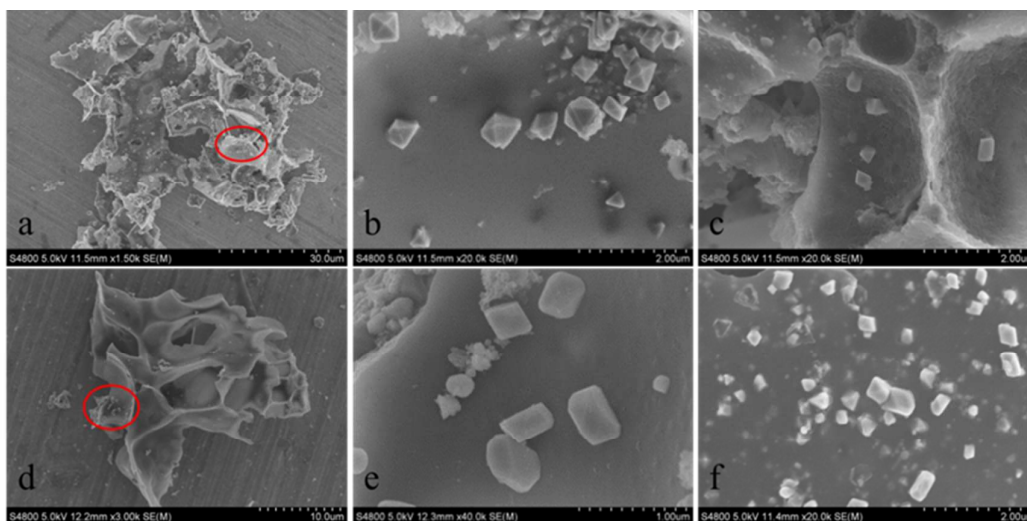


Fig. 1 SEM images of Fe<sub>3</sub>O<sub>4</sub>@C (a-c) and CuFe<sub>2</sub>O<sub>4</sub>/Cu@C (d-f).

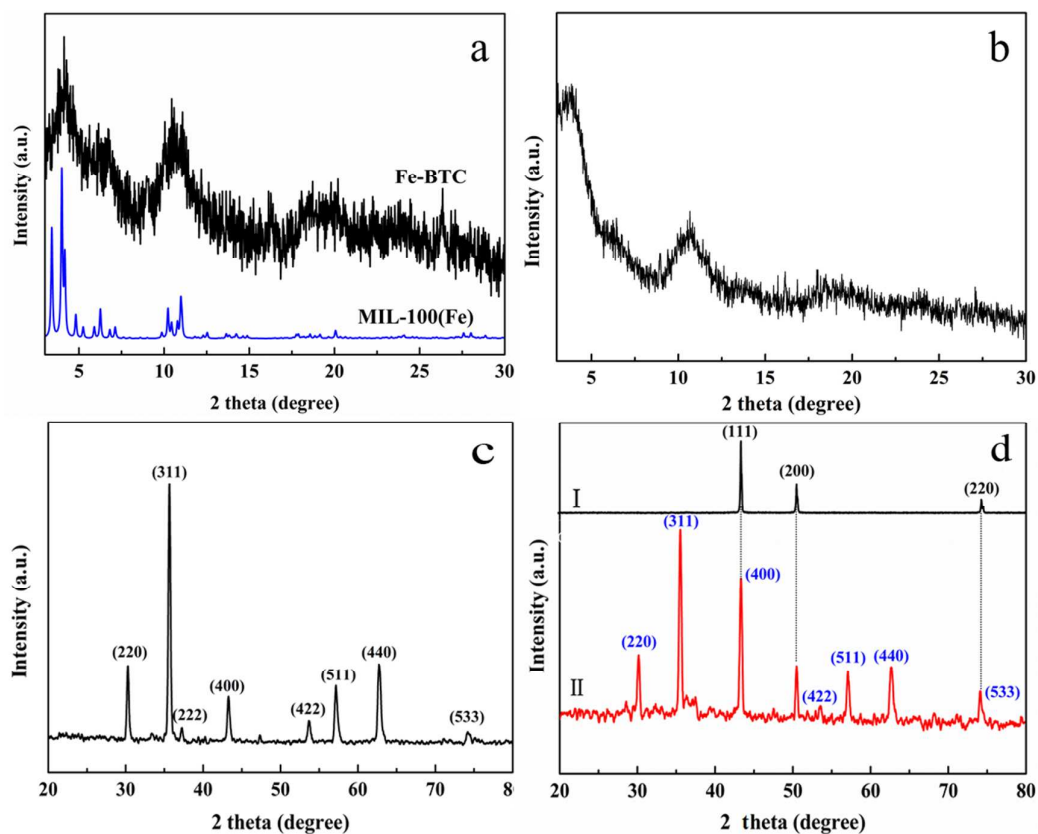


Fig. 2 XRD patterns of (a) Fe-BTC, (b) [Cu/Fe]-BTC, (c) Fe<sub>3</sub>O<sub>4</sub>@C and (d) CuFe<sub>2</sub>O<sub>4</sub>/Cu@C.

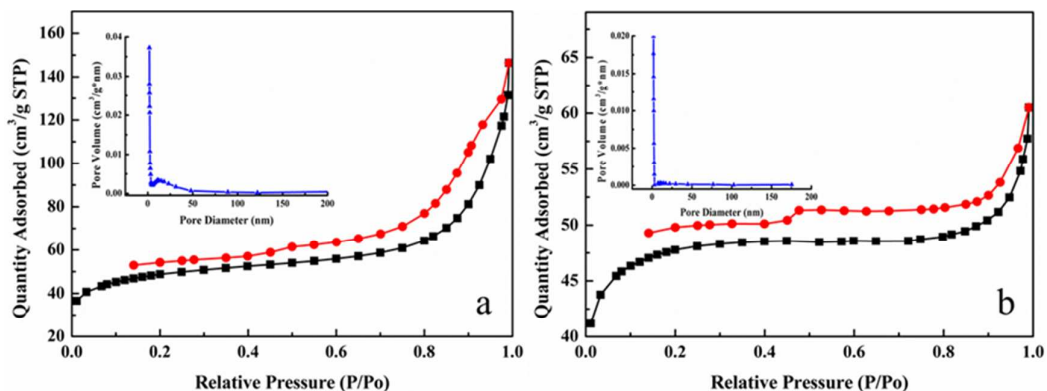


Fig. 3 N<sub>2</sub> adsorption-desorption isotherms of (a) Fe<sub>3</sub>O<sub>4</sub>@C and (b) CuFe<sub>2</sub>O<sub>4</sub>/Cu@C. the pore-size-distribution curve of (inset a) Fe<sub>3</sub>O<sub>4</sub>@C and (inset b) CuFe<sub>2</sub>O<sub>4</sub>/Cu@C obtained from the desorption data through the BJH method.

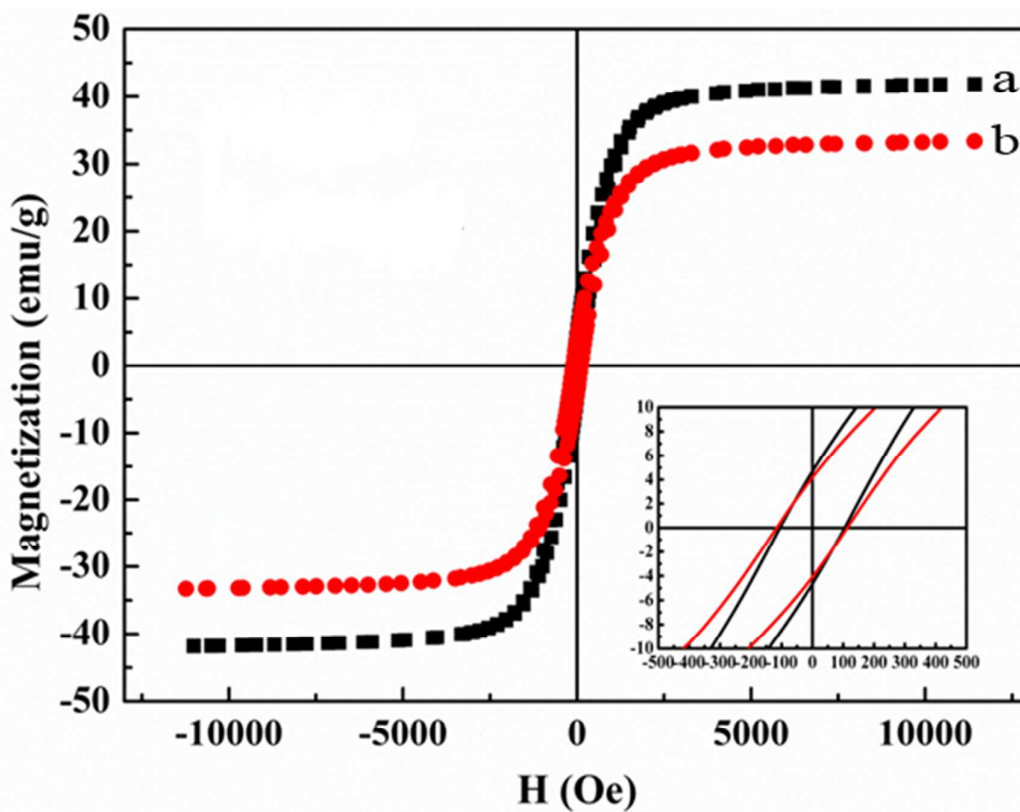


Fig. 4 Magnetic hysteresis loops of Fe<sub>3</sub>O<sub>4</sub>@C (a), and CuFe<sub>2</sub>O<sub>4</sub>/Cu@C (b). The inset is a magnified view of the magnetization versus field curves.

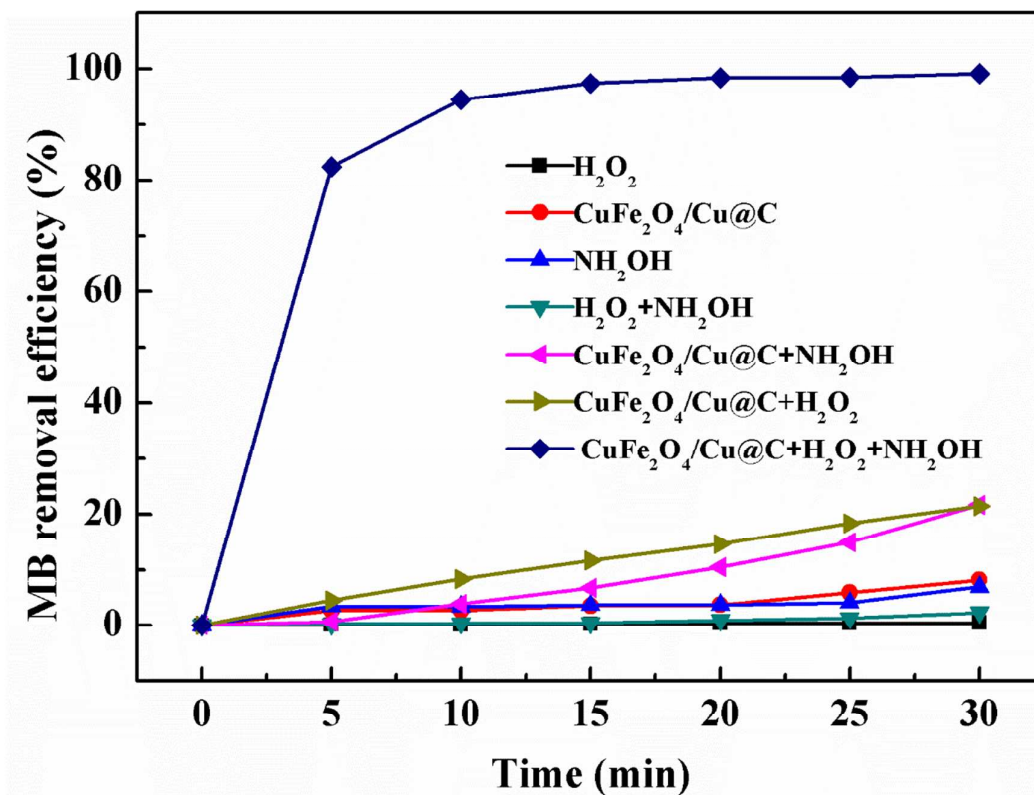


Fig. 5 Removal efficiency of MB under different conditions within 30 min. Reaction conditions: initial MB concentration,  $20 \text{ mg L}^{-1}$ ; initial  $\text{H}_2\text{O}_2$  concentration,  $16 \text{ mmol L}^{-1}$ ;  $\text{NH}_2\text{OH}$  concentration,  $4 \text{ mmol L}^{-1}$ ; catalyst load,  $0.5 \text{ g L}^{-1}$ ; initial solution pH, 7.0;  $T = 303 \text{ K}$ .

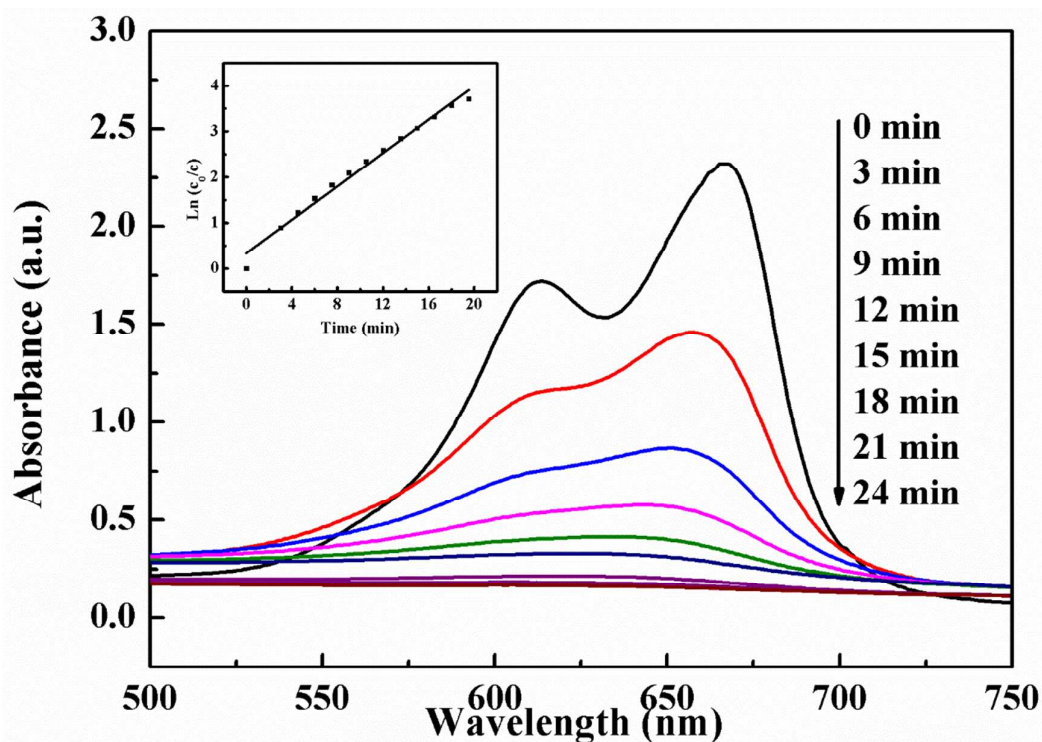


Fig. 6 UV-vis spectral changes of the 20 mg L<sup>-1</sup> MB solution in the degradation process as a function of the reaction time in the presence of 0.5 g L<sup>-1</sup> CuFe<sub>2</sub>O<sub>4</sub>/Cu@C, 6.67 mmol L<sup>-1</sup> NH<sub>2</sub>OH, and 5.33 mmol L<sup>-1</sup> H<sub>2</sub>O<sub>2</sub> at T = 303 K and pH 5.0. The inset Figure is First-order linear relationship.

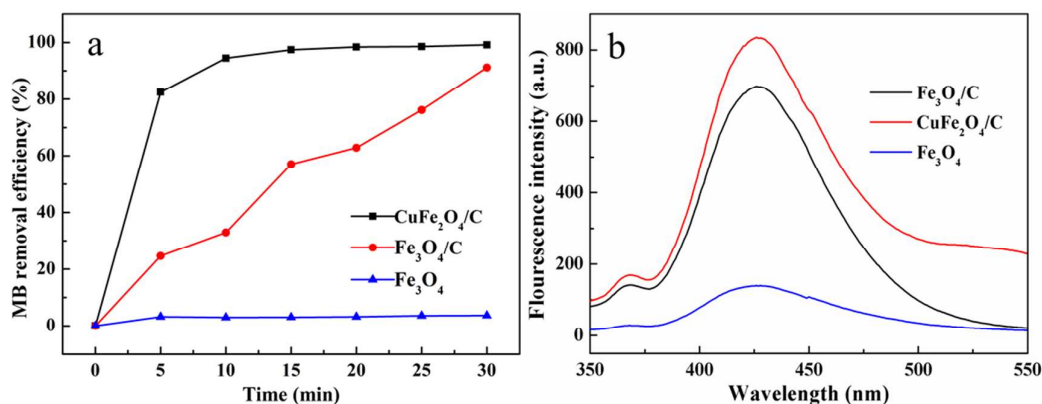


Fig. 7 Removal efficiency of MB under different catalysts (a), the dosage of HO• generated under different catalysts (b). conditions: (a) MB, 20 mg L<sup>-1</sup>; H<sub>2</sub>O<sub>2</sub>, 5.33 mmol L<sup>-1</sup>; NH<sub>2</sub>OH, 6.67 mmol L<sup>-1</sup>; catalysts, 0.5 g L<sup>-1</sup>; T = 303 K; pH 5.

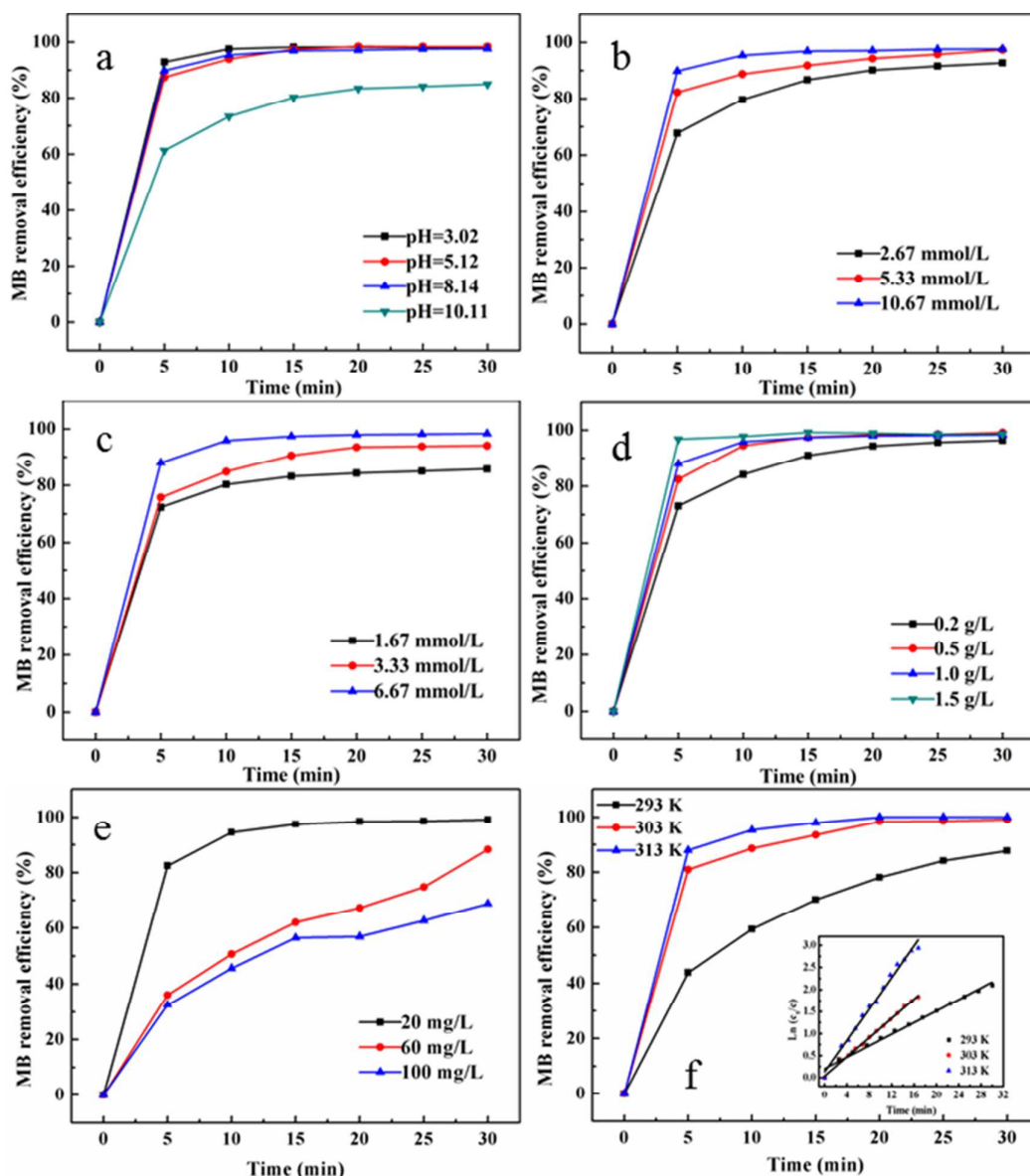


Fig. 8 Effect of the (a) pH, (b)  $\text{H}_2\text{O}_2$  concentration, (c)  $\text{NH}_2\text{OH}$  concentration, (d) dosage of the catalyst, (e) MB concentration, and (f) temperature conditions: (a) MB,  $20 \text{ mg L}^{-1}$ ;  $\text{H}_2\text{O}_2$ ,  $5.33 \text{ mmol L}^{-1}$ ;  $\text{NH}_2\text{OH}$ ,  $6.67 \text{ mmol L}^{-1}$ ;  $\text{CuFe}_2\text{O}_4/\text{Cu@C}$ ,  $0.5 \text{ g L}^{-1}$ ;  $T = 303 \text{ K}$ ; (b) MB,  $20 \text{ mg L}^{-1}$ ; pH, 5.0;  $\text{NH}_2\text{OH}$ ,  $6.67 \text{ mmol L}^{-1}$ ;  $\text{CuFe}_2\text{O}_4/\text{Cu@C}$ ,  $0.5 \text{ g L}^{-1}$ ;  $T = 303 \text{ K}$ ; (c) MB,  $20 \text{ mg L}^{-1}$ ;  $\text{H}_2\text{O}_2$ ,  $5.33 \text{ mmol L}^{-1}$ ; pH, 5.0;  $\text{CuFe}_2\text{O}_4/\text{Cu@C}$ ,  $0.5 \text{ g L}^{-1}$ ;  $T = 303 \text{ K}$ ; (d) MB,  $20 \text{ mg L}^{-1}$ ;  $\text{H}_2\text{O}_2$ ,  $5.33 \text{ mmol L}^{-1}$ ;  $\text{NH}_2\text{OH}$ ,  $6.67 \text{ mmol L}^{-1}$ ; pH, 5.0;  $T = 303 \text{ K}$ ; (e) pH, 5.0;  $\text{H}_2\text{O}_2$ ,  $5.33 \text{ mmol L}^{-1}$ ;  $\text{NH}_2\text{OH}$ ,  $6.67 \text{ mmol L}^{-1}$ ;  $\text{CuFe}_2\text{O}_4/\text{Cu@C}$ ,  $0.5 \text{ g L}^{-1}$ ;  $T = 303 \text{ K}$ ; (f) MB,  $20 \text{ mg L}^{-1}$ ;  $\text{H}_2\text{O}_2$ ,  $5.33 \text{ mmol L}^{-1}$ ;  $\text{NH}_2\text{OH}$ ,  $6.67 \text{ mmol L}^{-1}$ ;  $\text{CuFe}_2\text{O}_4/\text{Cu@C}$ ,  $0.5 \text{ g L}^{-1}$ ; pH, 5.0;

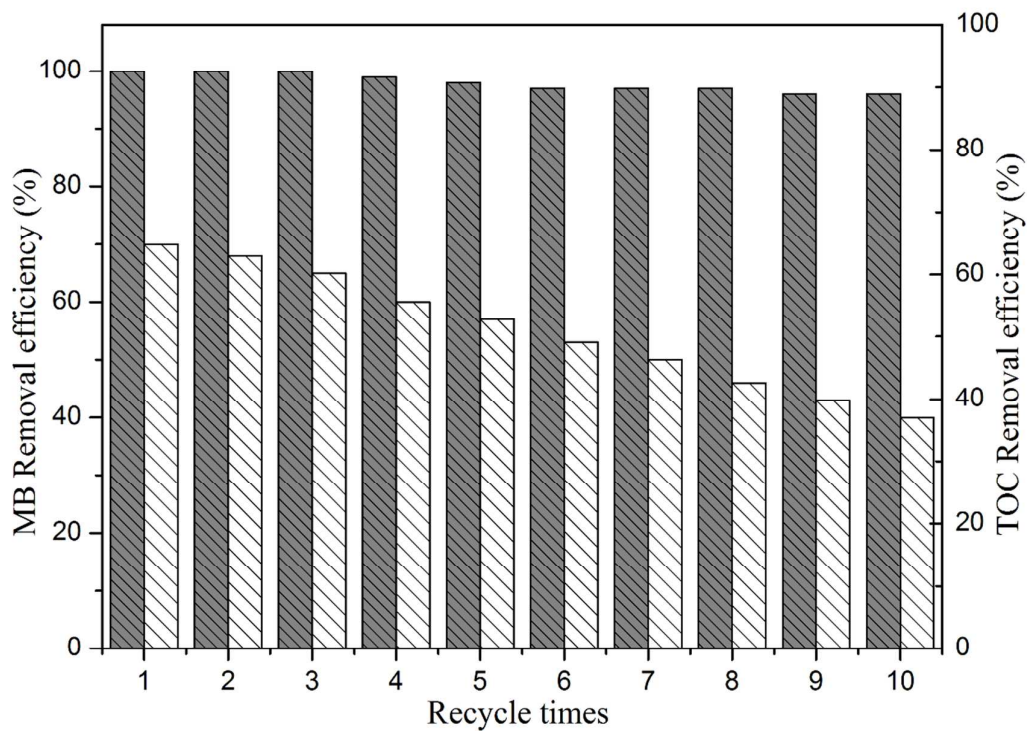


Fig. 9 Reuse of the catalyst. Reaction conditions: MB, 20 mg L<sup>-1</sup>; H<sub>2</sub>O<sub>2</sub>, 5.33 mmol L<sup>-1</sup>; NH<sub>2</sub>OH, 6.67 mmol L<sup>-1</sup>; CuFe<sub>2</sub>O<sub>4</sub>/Cu@C, 0.5 g L<sup>-1</sup>; T = 303 K; pH, 5

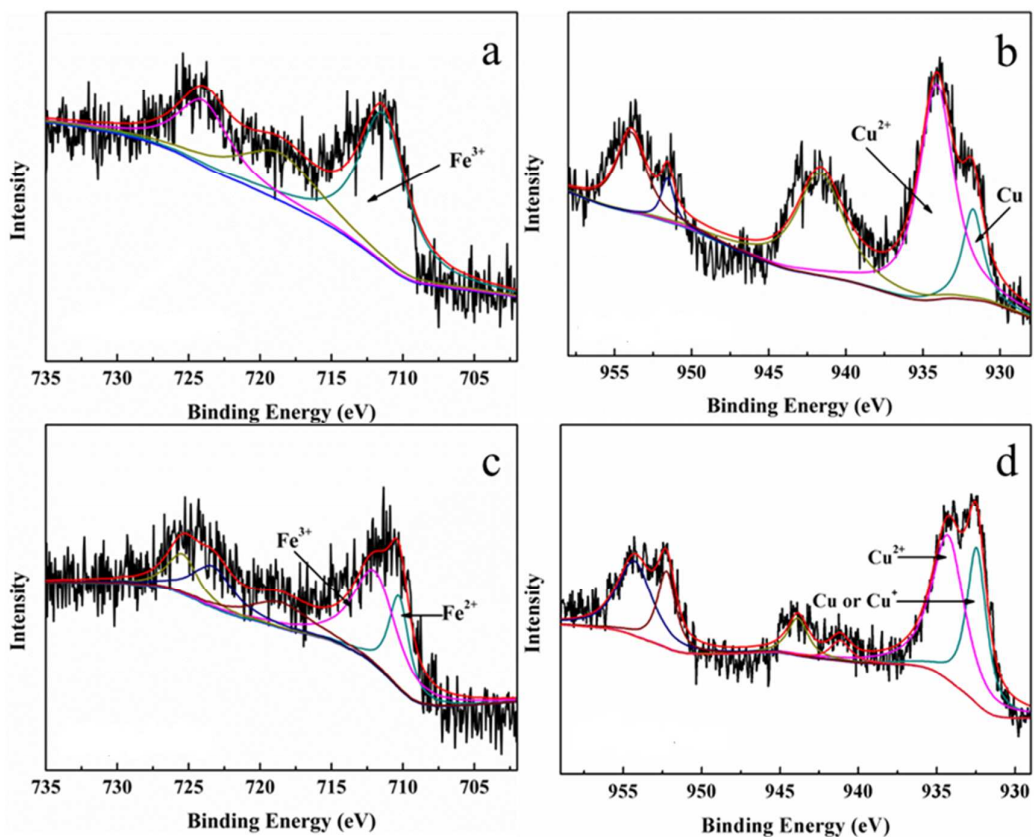


Fig. 10 XPS spectrum of iron before (a) and after (c) and copper before (b) and after (d) degradation of MB.

Table 1 Magnetic Properties of  $\text{Fe}_3\text{O}_4@\text{C}$  and  $\text{CuFe}_2\text{O}_4/\text{Cu}@\text{C}$

Samples	Magnetic Properties		
	$M_s$ (emu/g)	$H_c$ (Oe)	$M_R$ (emu/g)
$\text{Fe}_3\text{O}_4@\text{C}$	41.84	103	4.77
$\text{CuFe}_2\text{O}_4/\text{Cu}@\text{C}$	33.36	117	3.69

Table 2 The measured rate constants of MB degradation at different temperatures

T (K)	$\text{CuFe}_2\text{O}_4/\text{Cu}@\text{C}$	
	$k(\text{min}^{-1})$	$R^2$
293	0.06562	0.987
303	0.10942	0.998
313	0.17850	0.989

Table 3 XPS analysis of iron and copper on  $\text{CuFe}_2\text{O}_4/\text{Cu}@\text{C}$  before and after degradation of MB

		$\text{Fe}^{2+}$	$\text{Fe}^{3+}$	Cu	$\text{Cu}^+$	$\text{Cu}^{2+}$
binding energy (eV)	fresh	/	711.4	931.9	/	934.1
	used	710.3	711.9	931.9		934.3
The ratio of element valence state (%)	fresh	0	100	19.7	/	80.3
	used	31.4	68.6	39.4		60.6